



ARTICLE

Fusion of lysosomes to plasma membrane initiates radiation-induced apoptosis

Charles S. Ferranti^{1*}, Jin Cheng^{1*}, Chris Thompson², Jianjun Zhang¹, Jimmy A. Rotolo¹, Salma Buddaseth¹ , Zvi Fuks², and Richard N. Kolesnick¹ 

Diverse stresses, including reactive oxygen species (ROS), ionizing radiation, and chemotherapies, activate acid sphingomyelinase (ASMase) and generate the second messenger ceramide at plasma membranes, triggering apoptosis in specific cells, such as hematopoietic cells and endothelium. Ceramide elevation drives local bilayer reorganization into ceramide-rich platforms, macrodomains (0.5–5- μ m diameter) that transmit apoptotic signals. An unresolved issue is how ASMase residing within lysosomes is released extracellularly within seconds to hydrolyze sphingomyelin preferentially enriched in outer plasma membranes. Here we show that physical damage by ionizing radiation and ROS induces full-thickness membrane disruption that allows local calcium influx, membrane lysosome fusion, and ASMase release. Further, electron microscopy reveals that plasma membrane “nanopore-like” structures (\sim 100-nm diameter) form rapidly due to lipid peroxidation, allowing calcium entry to initiate lysosome fusion. We posit that the extent of upstream damage to mammalian plasma membranes, calibrated by severity of nanopore-mediated local calcium influx for lysosome fusion, represents a biophysical mechanism for cell death induction.

Introduction

There is consensus that lethal damage to mammalian cells by ionizing radiation occurs via induction of DNA double strand breaks (DSBs) that lead to mitotic death, and harnessing this principle for therapeutic benefit serves as a foundation of modern radiation therapy (Hall and Giaccia, 2012). However, evidence exists indicating that in a subset of cells, such as endothelium and hematopoietic cells, membrane damage rather than DNA damage signals cell death via apoptosis (Haimovitz-Friedman et al., 1994; Santana et al., 1996). Prior studies demonstrated that membrane-based apoptotic death requires activation of acid sphingomyelinase (ASMase), a lysosomal hydrolase that converts sphingomyelin to proapoptotic ceramide (Garcia-Barros et al., 2003; Santana et al., 1996; Seideman et al., 2011; Stancevic et al., 2013). Following diverse physical stress to plasma membrane, including reactive oxygen species (ROS), ionizing radiation, mechanical stress, and UV C, to list a few, ASMase is translocated within seconds to the cell surface of select cell types (Defour et al., 2014; Li et al., 2012; Rotolo et al., 2005, 2012). The substrate of ASMase, sphingomyelin, is preferentially concentrated in membrane rafts on the external leaflet of the plasma membrane (van der Goot and Harder, 2001) and is hydrolyzed therein by ASMase to

generate ceramide. Ceramide elevation above a cell type-specific membrane threshold drives coalescence of microscopic rafts into large macrodomains known as ceramide-rich platforms (CRPs; 0.5–5- μ m diameter) due to its high hydrophobicity, hydrogen bonding capability, and Van der Waal forces (Charruyer et al., 2005; Cremesti et al., 2001; Dumitru and Gulbins, 2006; Grassmé et al., 2002, 2003; Grassme et al., 2001; Rotolo et al., 2005, 2012; Seideman et al., 2011; Stancevic and Kolesnick, 2010; Stancevic et al., 2013). A set of membrane proteins insert into these platforms and oligomerize therein, facilitating transmembrane stress signal transduction (Cremesti et al., 2001; Dumitru and Gulbins, 2006; Grassmé et al., 2002, 2003; Grassme et al., 2001). In hematopoietic cells and endothelium, this process appears requisite for maximal apoptosis in response to ionizing radiation stress (Rotolo et al., 2012; Santana et al., 1996; Stancevic et al., 2013; Truman et al., 2010). The current study identifies the physical radiation injury to membranes that initiates lysosomal ASMase release to the extracellular space, the proximal event in this cell death cascade.

Our studies reported here draw on recent data from the Norma Andrews group (Idone et al., 2008; Tam et al., 2010)

¹Laboratory of Signal Transduction, Memorial Sloan-Kettering Cancer Center, New York, NY; ²Department of Radiation Oncology, Memorial Sloan-Kettering Cancer Center, New York, NY.

*C.S. Ferranti and J. Cheng contributed equally to this paper; Correspondence to Richard Kolesnick: r-kolesnick@ski.mskcc.org; J. Zhang's present address is Department of Thoracic/Head and Neck Medical Oncology, MD Anderson Cancer Center, Houston, TX; J.A. Rotolo's present address is Sapience Therapeutics, Harrison, NY.

© 2020 Ferranti et al. This article is distributed under the terms of an Attribution–Noncommercial–Share Alike–No Mirror Sites license for the first six months after the publication date (see <http://www.rupress.org/terms/>). After six months it is available under a Creative Commons License (Attribution–Noncommercial–Share Alike 4.0 International license, as described at <https://creativecommons.org/licenses/by-nc-sa/4.0/>).

showing that exposure of normal rat kidney epithelial cells to the bacterial toxin streptolysin-O (SLO) injures the cell membrane by forming transmembrane channels. Subsequent calcium influx leads to exocytosis of ASMase-containing lysosomes by their fusion with the injured plasma membrane, and newly generated ceramide at the cell surface promotes endocytosis of the toxin by inward rectification of the plasma membrane (Idone et al., 2008; Tam et al., 2010), a biophysical property of asymmetric ceramide content within a bilayer (Holopainen et al., 2000; Nurminen et al., 2002). The ultimate biological outcome of this ASMase secretion response to SLO toxin is removal of toxin and the damaged portion of plasma membrane by endocytosis, rendering membrane resealing and cell survival. We hypothesized that physical damage to the plasma membrane bilayer by ionizing radiation might induce a similar calcium-dependent ASMase secretion via lysosomal exocytosis that will yield apoptotic lethality rather than membrane repair.

Here we demonstrate that clinically relevant doses of ionizing radiation and H₂O₂ induce transient bidirectional disruption of plasma membrane barrier function mediated by oxidative damage of membrane lipids. This damage enables extracellular calcium to flow down its concentration gradient into the sub-membrane space, eliciting lysosome fusion, ASMase release, and generation of CRPs for apoptosis induction. Further, we report the discovery of well-circumscribed “nanopore-like” structures (~100-nm diameter) that appear within seconds in plasma membrane following radiation and H₂O₂ exposure, and we provide evidence that these structures represent full-thickness disruptions of the bilayer, which facilitate the calcium influx required for lysosome fusion.

Results

ASMase mediates ionizing radiation-induced apoptosis in Jurkat T cells

ASMase activation signals radiation-induced apoptotic cell death in the endothelium of diverse tissues and tumors, and in hematopoietic systems (Garcia-Barros et al., 2003; Rotolo et al., 2012; Santana et al., 1996; Seideman et al., 2011; Stancevic et al., 2013). The current studies use human Jurkat T lymphocytes, frequently used to model this ASMase-dependent apoptotic biology (Cremesti et al., 2001; Grassme et al., 2001; Rotolo et al., 2005; Seideman et al., 2011). Numerous reports highlight the downstream apoptotic effectors following exposure of Jurkat cells to ionizing radiation, which include caspase activation, Bid (BH3-interacting domain death agonist) cleavage, and mitochondrial outer membrane permeabilization (Belka et al., 1999, 2003; Boesen-de Cock et al., 1999; Tepper et al., 1999). Fig. 1 A shows that at 10 Gy, the maximal dose for ceramide-dependent apoptosis induction in Jurkat T cells (Fig. 1 F), ASMase is rapidly translocated to the external plasma membrane, detectable within 30 s, and peaking at 2 min, as visualized by confocal microscopy. ASMase on the surface of irradiated cells was detected using rabbit polyclonal 1598 anti-human ASMase antibody, as published (Rotolo et al., 2005; Stancevic et al., 2013). As little as 2 Gy induced ASMase release into the cell medium by 1 min, an event that peaked at 10 Gy, detected by standard

radioenzymatic assay using [¹⁴C]sphingomyelin as substrate (Rotolo et al., 2005; van Hell et al., 2017; Fig. 1 B). Ceramide, the product of ASMase hydrolysis of sphingomyelin on the external plasma membrane, is detectable by 30 s and peaks at 5 min (Fig. 1 C), associated with CRP formation on the outer membrane as detected by staining with MID 15B4 anti-ceramide monoclonal antibody (Rotolo et al., 2005, 2012; Stancevic et al., 2013; Fig. 1 D). Radiation subsequently induced time-dependent (Fig. 1 E) and dose-dependent (Fig. 1 F) Jurkat cell apoptosis, an event inhibitable by humanized 2A2 (h2A2) anti-ceramide antibody (Fig. 1 G). Note that, at doses >10 Gy, DNA damage-dependent apoptotic death of Jurkat cells occurred, which is not inhibitable by anti-ceramide antibody (Fig. S1 A). Radiation-induced CRP formation and apoptotic death at 10 Gy were similarly inhibited by 1-h preincubation with imipramine, which promotes rapid ASMase degradation within lysosomes by displacing ASMase from its binding partner, bis(monoacylglycerol)phosphate, on the inner lysosomal membrane (Beckmann et al., 2014; Fig. S1 B). These studies indicate that ionizing radiation induces ASMase/ceramide-dependent apoptotic death of Jurkat T cells that is comparable to that induced in endothelial and lymphoblastic cell lines in culture (Verheij et al., 1996; Vit and Rosselli, 2003), and in vivo in the microvasculature of the small intestine and multiple types of tumor xenografts (Garcia-Barros et al., 2003; Stancevic et al., 2013).

ASMase response to ionizing radiation is dependent on extracellular calcium influx

While little is known regarding the mechanism by which lethal stresses induce ASMase secretion within seconds, evidence indicates that extracellular calcium influx is requisite for SLO-induced lysosome fusion with plasma membrane, with consequent release of ASMase (and other lysosomal hydrolases) to the external plasma membrane (Tam et al., 2010). To examine the impact of extracellular calcium depletion on radiation-induced ASMase secretion, we resuspended Jurkat cells in RPMI 1640 without calcium supplemented with 2 mM EGTA, an established approach to studying the potential role of calcium influx in biological processes (Idone et al., 2008; Reddy et al., 2001; Tam et al., 2010). Removal of extracellular calcium blocked radiation-induced ASMase surface translocation (Fig. 2 A). Consistent with fusion of lysosomes with plasma membrane as the source of ASMase release, we showed that lysosome-associated membrane protein 1 (LAMP1), an established marker of lysosome fusion with plasma membrane, was detected by 1 min after 10 Gy on the surface of Jurkat T cells, as analyzed by confocal microscopy (Fig. 2 B). Surface LAMP1 peaks by 5 min at a level ~15-fold that of unirradiated cells. Lysosome fusion with plasma membrane as detected by the appearance of LAMP1 was markedly inhibited by removal of extracellular calcium (Fig. S2), consistent with calcium influx mediating ASMase secretion after irradiation.

To further confirm that calcium flux is required for this ASMase response, cells were preloaded with 10 μM 1,2-bis(2-aminophenoxy)ethane-*N,N,N',N'*-tetraacetic acid tetrakis(acetoxymethyl) ester (BAPTA-AM) to chelate potential elevation in cytoplasmic free calcium, as described (Czibener et al., 2006). Consistent with calcium influx mediating ASMase secretion via lysosome fusion with plasma membrane, BAPTA-AM was

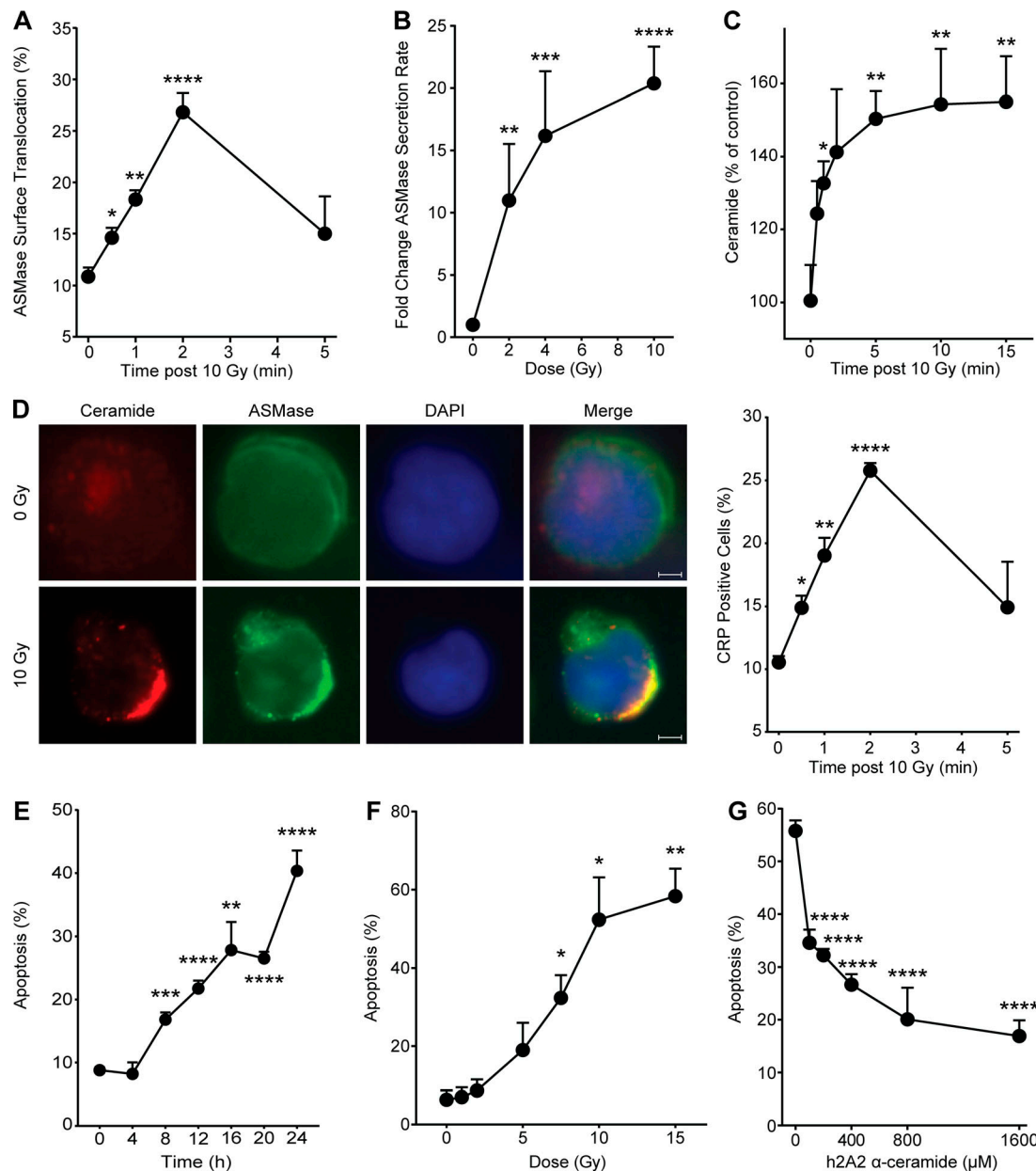


Figure 1. Ionizing radiation induces ASMase secretion in Jurkat T lymphocytes. (A) ASMase surface translocation following 10-Gy exposure quantified by percentage of cell population demonstrating surface staining by anti-ASMase antibody. (B) Secreted ASMase enzymatic activity detected in cleared cell medium 1 min following escalating doses of ionizing radiation using [14 C]sphingomyelin as substrate. (C) Time course of ceramide generation detected by diacylglycerol kinase assay following 10-Gy exposure. (D) Representative fluorescence microscopy images of ceramide (red) and ASMase (green) surface staining following 10-Gy exposure (colocalization [yellow], DAPI counterstain; left). Scale bars: 3 μ m. CRP formation following exposure to 10 Gy, quantified as percentage of cell population featuring platforms stained with anti-ceramide antibody (right). (E) Time course of apoptosis following exposure to 10 Gy, detected by bisbenzimidazole (Hoechst #33258) nuclear staining. Data (mean \pm SEM) are derived from five representative fields per group. (F) Apoptosis dose response 24 h after irradiation detected by bisbenzimidazole nuclear staining. (G) Protection against 10 Gy-induced apoptosis by pretreatment with h2A2 anti-ceramide antibody detected by bisbenzimidazole nuclear staining. Data (mean \pm SD) are from a minimum of 500 cells per group. In A–D and F, data represent mean \pm SEM collated from three independent experiments. *, $P < 0.05$; **, $P < 0.01$; ***, $P < 0.001$; ****, $P < 0.0001$, two-tailed Student's t test versus respective control time zero (A, C, D, and E), 0 Gy (B and F), or 0 μ M (G).

sufficient to block lysosomal exocytosis, as measured by β -hexosaminidase release (Fig. 2 C). Furthermore, removal of extracellular calcium inhibited formation of CRPs (Fig. 2 D). Similarly, BAPTA-AM pretreatment completely blocked radiation-induced ASMase secretion into cell medium following 10 Gy (Fig. 2 E) and reduced radiation-induced apoptosis

(Fig. 2 F). Bromoenol lactone (BEL), an inhibitor of calcium-dependent lysosomal fusion with plasma membrane (Tam et al., 2010), also inhibited both radiation-induced LAMP1 surface staining and apoptosis (Fig. S1, C and D), consistent with localized calcium influx triggering lysosome fusion to mediate ASMase release and initiate apoptosis.

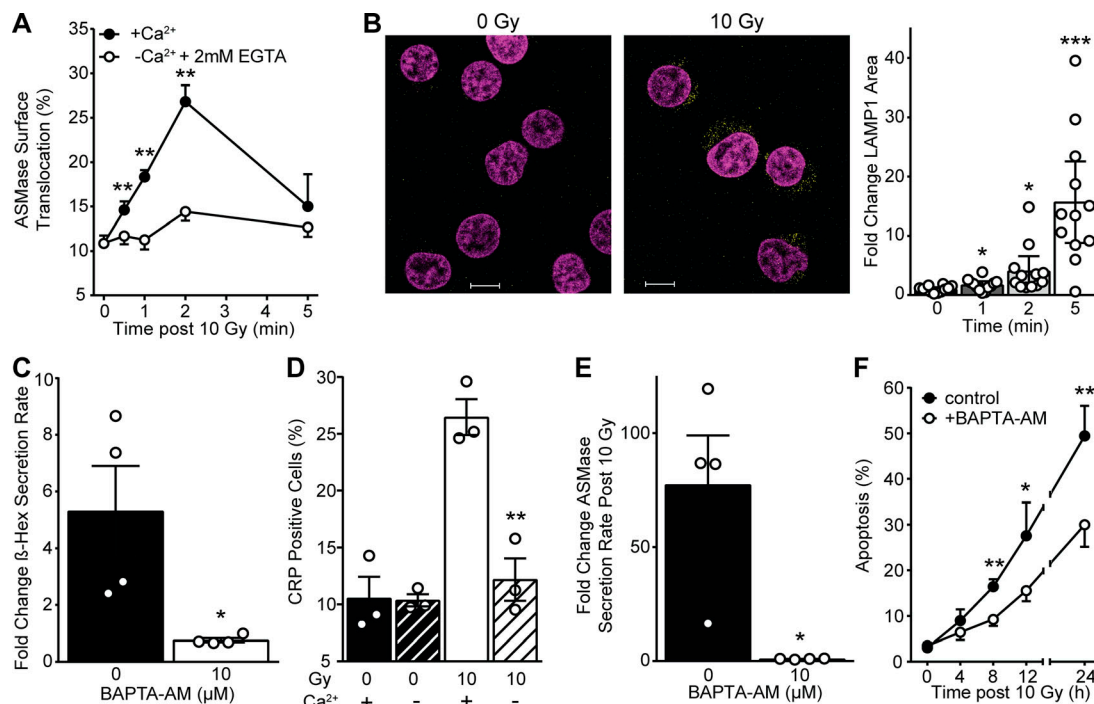


Figure 2. Calcium-dependent lysosomal fusion with the plasma membrane mediates ionizing radiation-induced ASMase secretion and apoptosis. (A) 10 Gy-induced ASMase surface translocation measured using anti-ASMase antibody is inhibited by removal of extracellular calcium and supplementation with 2 mM EGTA. Controls with calcium are the same as those in Fig. 1 A. (B) Representative confocal fluorescence microscopy images of LAMP1 (yellow) surface staining using anti-LAMP1 antibody following 10 Gy (DAPI counterstain [magenta], left) and quantification (right). Scale bars: 10 μm. Data (mean ± 95% confidence interval) are derived from 12 cells per group. This experiment was performed four times with similar results. (C) Secreted β-hexosaminidase activity detected in cleared cell medium 2 min following 10 Gy with and without BAPTA-AM pretreatment. (D) 10 Gy-induced CRP formation 2 min after ionizing radiation as measured by anti-ceramide surface staining is inhibited by removal of extracellular calcium with EGTA supplementation. (E) Secreted ASMase activity detected in cleared cell medium using [¹⁴C]sphingomyelin substrate at 2 min following 10-Gy exposure is abrogated by BAPTA-AM pretreatment. (F) Apoptosis quantified by bisbenzimidazole nuclear staining following 10 Gy is diminished following BAPTA-AM pretreatment. Data (mean ± SD) are from five representative fields per group. In A and C–E, data represent mean ± SEM collated from three to four independent experiments; for A–F, *, $P < 0.05$; **, $P < 0.01$; ***, $P < 0.001$, two-tailed Student's *t* test versus $-Ca^{2+}$ (A), 0 min (B), 0 mM BAPTA-AM (C and E), 10 Gy (D), or +BAPTA-AM (F).

Ionizing radiation induces disruption of the plasma membrane

To investigate whether the calcium-dependent ASMase response to ionizing radiation is triggered by permeabilization of the plasma membrane, we initially examined propidium iodide (PI) uptake as a measure of plasma membrane integrity. In unirradiated cells, $3.9 \pm 1.4\%$ (mean ± SEM) of the population displays PI uptake, increasing fourfold to $15.6 \pm 1.9\%$ (mean ± SEM) 10 min after 10 Gy (Fig. 3 A). However, as PI is traditionally used as a measure of cytotoxicity, it is relatively insensitive to sublethal damage and hence would likely underrepresent rapidly repaired plasma membrane permeabilization induced by irradiation. To further scrutinize radiation-induced plasma membrane permeabilization, we examined uptake of the lipophilic dye FM 1-43 (*N*-(3-triethylammoniumpropyl)-4-(4-(dibutylamino) styryl) pyridinium dibromide), standardized as a measure of membrane integrity (Howard et al., 2011; Tam et al., 2013). While FM 1-43 loads effectively into plasma membrane (Fig. 3 B, 0 Gy), it does not spontaneously disperse into the cytoplasmic compartment for ≥10 min. However, by 30 s after irradiation, FM 1-43 rapidly disperses throughout the cytoplasm, increasing 44-fold therein (Fig. 3 B, 10 Gy). A possible source of this increase in intracellular fluorescence is the endocytosis of dye present in the plasma membrane. To ensure that the observed increase is not due to dye endocytosis, we performed the same

experiment in the presence of the small molecule pitstop 2, originally designed as a specific inhibitor of clathrin but subsequently reported to inhibit both clathrin-mediated and -independent endocytosis (Dutta et al., 2012). Pitstop 2 treatment did not inhibit radiation-induced uptake of FM 1-43, suggesting that endocytosis is not the source of dye uptake (Fig. S3 A). However, removal of FM 1-43 from the medium immediately before irradiation, which did not impact membrane distribution of FM 1-43, resulted in complete loss of dye uptake (Fig. S3 B), indicating that the source of the rapid diffusion of FM 1-43 throughout intracellular membranous compartments is not derived from plasma membrane but rather from the extracellular space. Note that this plasma membrane disruption represents sublethal damage, as it occurs within seconds to minutes following radiation exposure, hours before lethal effects of radiation are observed.

Ionizing radiation-induced plasma membrane permeabilization was further demonstrated by release of chromium-51 from prelabeled cells. Release of Cr-51 was detected in cell buffer within minutes of exposure to 10 Gy ($28.2 \pm 0.5\%$ compared with control; mean ± SEM) and escalated in a dose-dependent manner up to 40 Gy (Fig. 3 C). In an approach complementary to Cr-51 release, we measured release of lactate dehydrogenase (LDH), a cytoplasmic protein of 144 kD accepted as a detector of

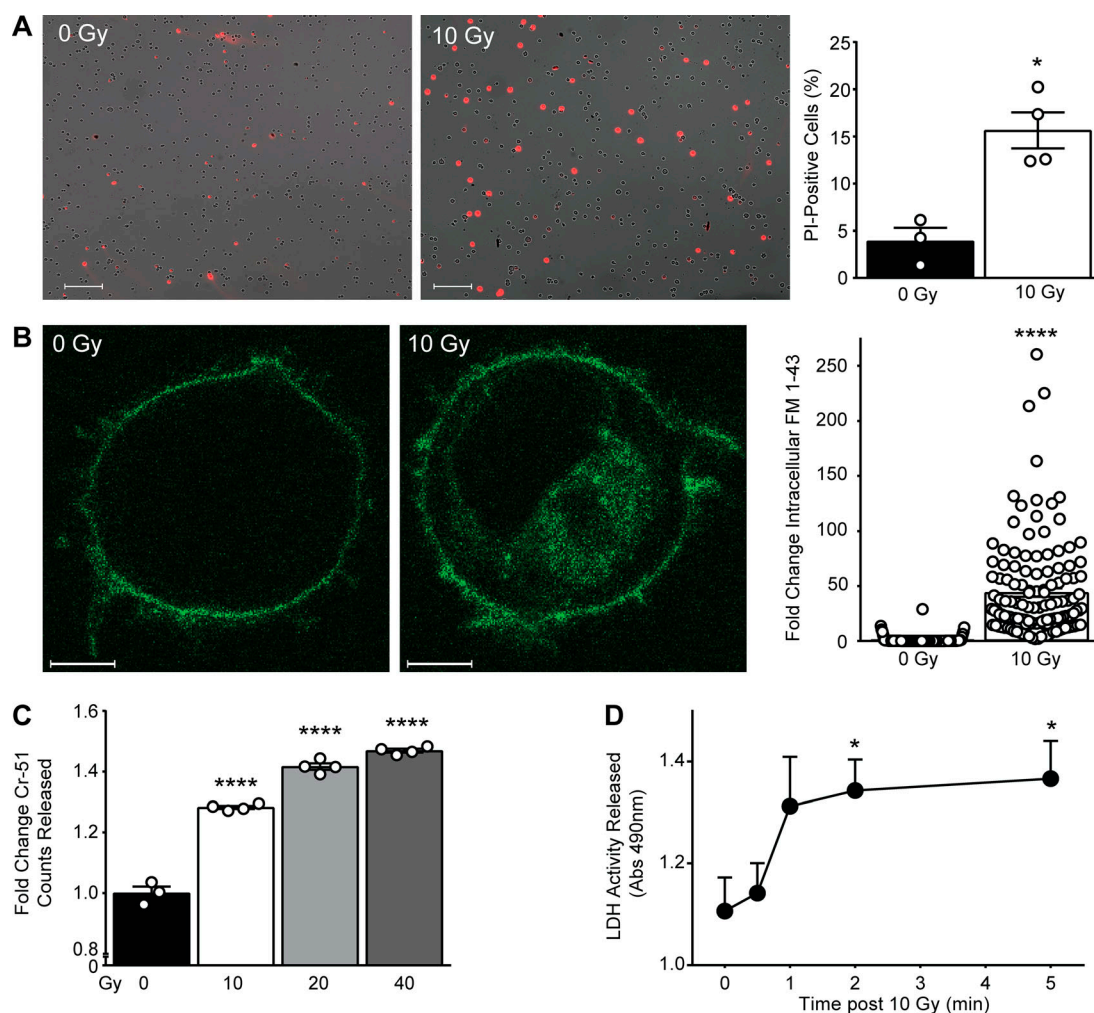


Figure 3. Ionizing radiation induces plasma membrane permeabilization. (A) Representative merged fluorescence and bright-field microscopy images of PI (red) cellular uptake immediately following 10 Gy (left), quantified as percentage of cells featuring PI signal (right). Data are from three to four representative images counted per group. This experiment was repeated twice with similar results. Scale bars: 100 μ m. (B) Representative confocal fluorescence microscopy images of FM 1-43 dye (green) uptake by 10 min following 10 Gy (left), quantified as fold change intracellular integrated density (right). Data are from a minimum of 100 cells per group. This experiment was repeated three times with similar results. Scale bars: 3 μ m. (C) Chromium-51 release measured from cleared cell buffer following escalating doses of ionizing radiation. Data are from three technical replicates. This experiment was repeated twice with similar results. (D) LDH release in cleared cell medium following 10 Gy exposure. Abs, absorbance. Data are collated from three to four independent experiments. In A–D, data represent mean \pm SEM; *, $P < 0.05$; ****, $P < 0.0001$, two-tailed Student's t test versus respective control 0 Gy (A–C) or 0 min (D).

transmembrane cellular damage (Reddy et al., 2001). Notably, it has been observed that release of preloaded Cr-51 and endogenous LDH correlate following various injurious stimuli (Bordenave et al., 1993). In Jurkat cells irradiated with 10 Gy, LDH release demonstrates cell permeabilization that plateaus by 2 min after irradiation (Fig. 3 D), suggesting temporary damage that is rapidly rectified. Altogether, these data indicate interruption of membrane barrier function, as demonstrated by bi-directional flow of various probes that occurs within seconds to minutes of radiation exposure, placing it within the known time frame of radiation-induced ASMase activity.

Role of ionizing radiation-induced oxidative damage to plasma membrane

It is widely accepted that damaging effects of ionizing radiation in mammalian cells under normoxic conditions result in part

from radiolysis of water rendering oxidative stress via generating ROS, which mediate radiation damage to DNA (Hall and Giaccia, 2012; LeMotte and Little, 1984; Radford and Hodgson, 1985). To determine whether the plasma membrane ASMase response to ionizing radiation is also oxidation dependent, we employed the well-described aqueous antioxidant 4-hydroxy-2,2,6,6-tetramethylpiperidin-1-oxyl (TEMPOL; Hahn et al., 1994). Pretreating cells for 30 min with 10 mM TEMPOL reduced both radiation-induced CRP formation at 2 min and apoptosis at 16 h following 10 Gy, suggesting that TEMPOL protects cells against radiation-induced ASMase-dependent apoptotic death via inhibition of oxidative damage (Fig. 4, A and B). To model the impact of ionizing radiation-induced ROS, we employed H_2O_2 as a source of oxidative damage. Notably, ASMase activity and lysosomal exocytosis in response to H_2O_2 has been previously reported in Jurkat cells (Li et al., 2012). Apoptosis

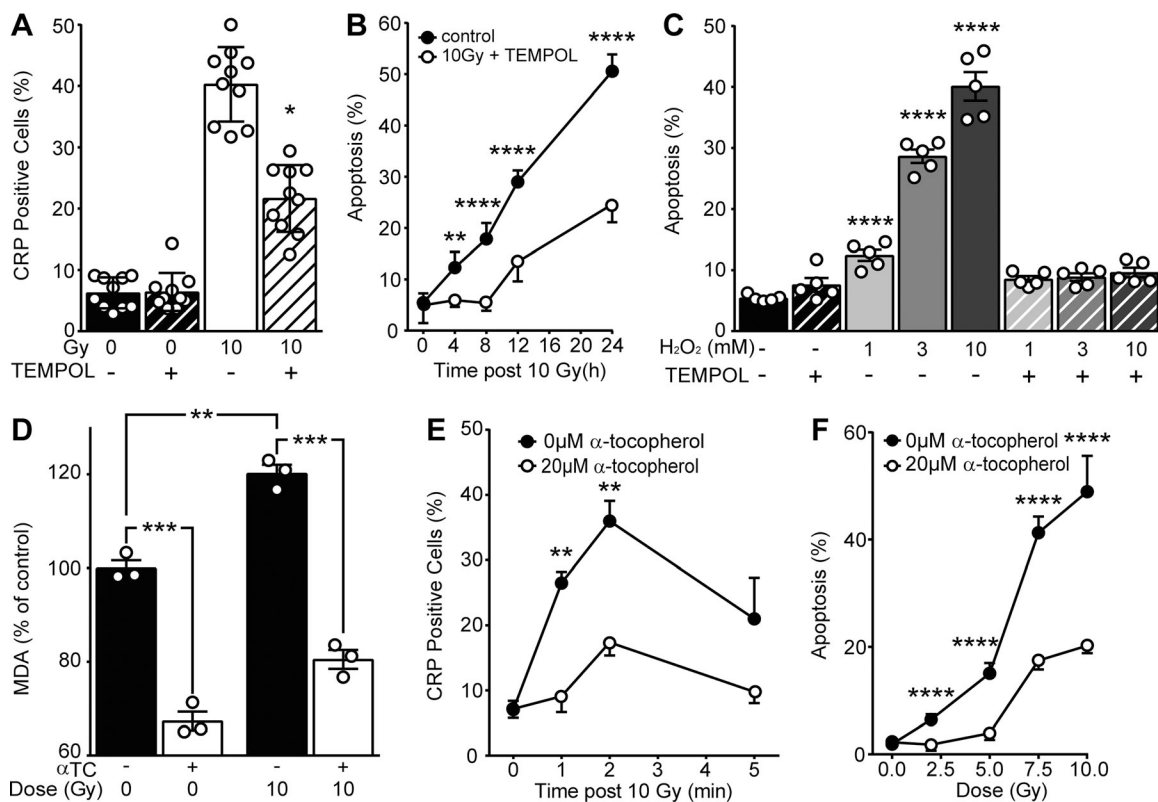


Figure 4. Ionizing radiation-induced oxidative stress facilitates ASMAse activation and apoptosis. (A) 20-mM TEMPOL pretreatment inhibits CRP formation detected 2 min after 10 Gy using anti-ceramide antibody. Data are from 10 representative fields per group. (B) Pretreatment with TEMPOL inhibits apoptosis following 10 Gy, detected by bisbenzamide nuclear staining. (C) TEMPOL pretreatment abolishes 5-min H₂O₂ treatment-induced apoptosis measured at 24 h. (D) α-Tocopherol pretreatment blocks 10 Gy-induced lipid peroxidation as assayed by MDA formation. Data are from three technical replicates. This experiment was repeated three times with similar results. (E) α-Tocopherol pretreatment inhibits 10 Gy-induced CRP formation as detected by anti-ceramide antibody. (F) α-Tocopherol pretreatment reduces ionizing radiation-induced apoptosis at 16 h. Data represent mean ± SD (A, B, and F) and mean ± SEM (C–E) from five representative fields (C and F) and three to four collated experiments (B and E). *, $P < 0.05$; **, $P < 0.01$; ***, $P < 0.001$; ****, $P < 0.0001$, two-tailed Student's *t* test versus 10 Gy (A), +TEMPOL (B), 0 mM H₂O₂ (C), as indicated (D), or 20 μM α-tocopherol (E and F).

following exposure of up to 10 mM H₂O₂ was completely inhibited by TEMPOL (Fig. 4 C). Furthermore, as radiation is known to induce oxidative damage to plasma membrane lipids (Stark, 1991), we quantified lipid peroxidation using malondialdehyde (MDA), a stable end product of lipid peroxidation chain reactions (Stark, 1991), and used the lipophilic antioxidant α-tocopherol (Vitamin E; Howard et al., 2011) to protect plasma membrane from this damage. At 20 μM α-tocopherol, both baseline MDA levels and radiation-induced MDA elevations were significantly reduced, indicating effective inhibition of lipid peroxidation (Fig. 4 D). Importantly, 20 μM α-tocopherol significantly reduced radiation-induced ceramide signaling, as evidenced by a reduced number of CRP-forming irradiated Jurkat T cells (Fig. 4 E), and apoptotic cell death (Fig. 4 F). These data indicate that ionizing radiation-induced oxidation of membrane lipids, and not radiation-induced DNA damage, yields ASMAse/ceramide signaling of apoptotic death.

Visualization of radiation-induced plasma membrane damage

Finally, in an effort to delineate the mechanism of ionizing radiation-induced plasma membrane permeabilization, we examined the surface of irradiated Jurkat cells in the time frame (seconds to minutes) of ASMAse activation by scanning electron

microscopy to visualize alterations in membrane structure. Note that the surface of a Jurkat cell under resting conditions is smooth and contains a plethora of fimbriae-like structures (Fig. 5 A, left). After 10 Gy, numerous membrane disruptions rapidly appear on the surface, with a mean diameter of 121.5 ± 2.6 nm (mean ± SEM; Fig. 5 A, right). Membrane disruptions display distinct features, often being ovoid and exhibiting a puckered contrast-enhanced perimeter (Fig. 5 B). The number of disruptions increases linearly with dose ($R^2 = 0.9850$) at 1 min up to 40 Gy (Fig. 5 C), and kinetic analysis reveals that these disruptions peak at 1 min after 10 Gy and dissipate thereafter (Fig. 5 D). We termed these disruption structures nanopore-like due to their nanometer-scale diameter. Importantly, 20 μM α-tocopherol significantly reduced radiation-induced nanopore formation (Fig. 5 E). Radioprotection by α-tocopherol and other vitamin E analogues against apoptotic death has been previously described (Singh et al., 2013). These studies suggest a fundamental role for lipid peroxidation in radiation-induced nanopore formation, upstream of cell death.

Subsequent studies used H₂O₂ to investigate the impact of ROS on plasma membrane structure. Following 1 mM H₂O₂, we observed formation of nanopore-like structures on the surface of Jurkat T cells that were morphologically indistinguishable

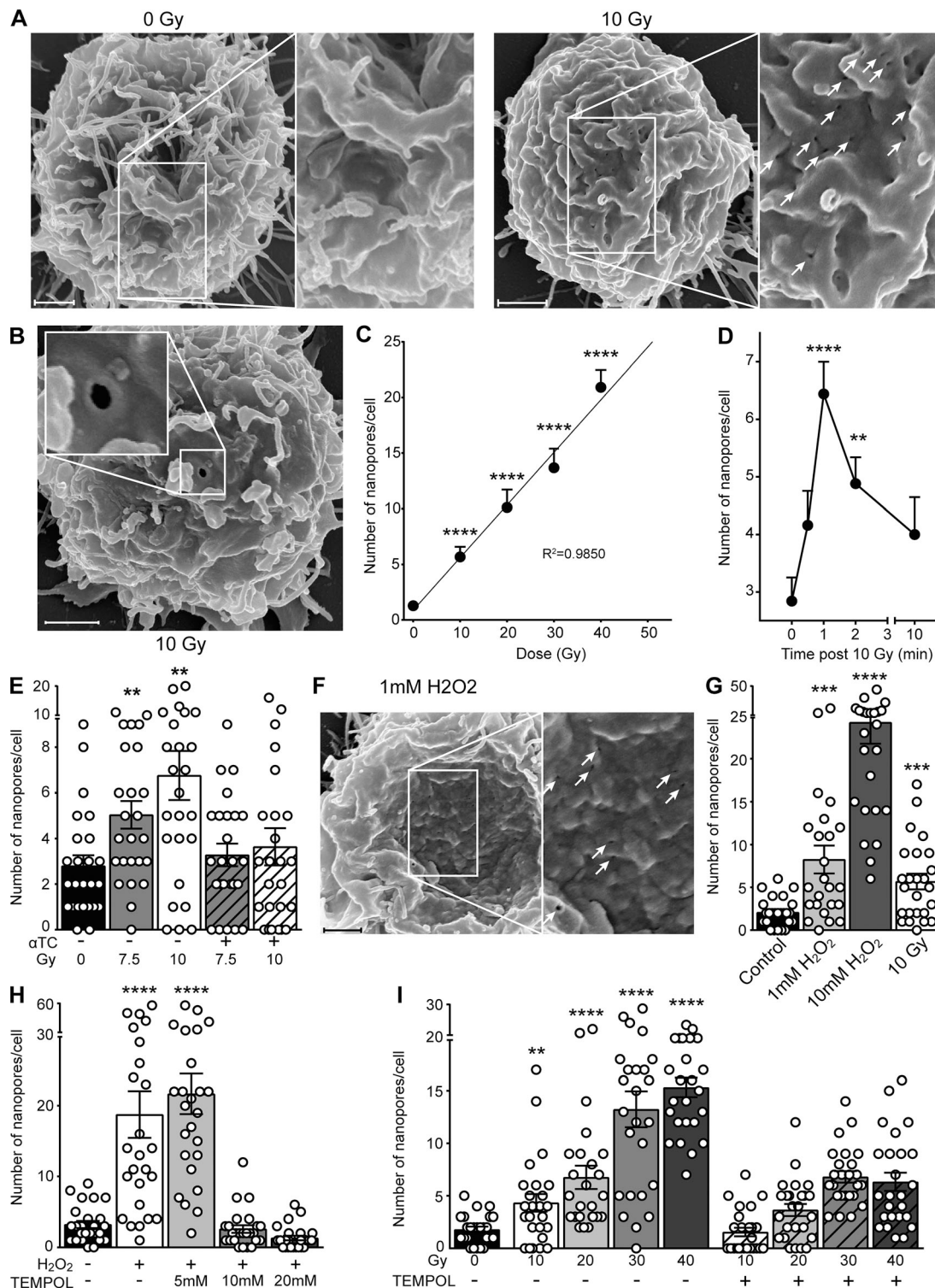


Figure 5. Plasma membrane nanopore formation following exposure to ionizing radiation and H₂O₂. (A and B) Representative scanning electron micrographs of plasma membrane nanopores (unirradiated control [A, left], white arrows on right [A], inset in B) 1 min following 10-Gy exposure. (C) Nanopore formation 1 min following ionizing radiation exposure is linear up to 40 Gy, quantified from scanning electron micrographs. (D) Time course of nanopore formation following exposure to 10 Gy, quantified from scanning electron micrographs. (E) α -Tocopherol pretreatment abrogates ionizing radiation-induced nanopore formation as quantified from scanning electron micrographs. (F) Representative scanning electron micrograph of plasma membrane nanopores (white arrows) 1 min following H₂O₂ exposure. (G) Comparison of nanopore formation following H₂O₂ and 10-Gy ionizing radiation exposure. The 10-Gy group is the same as that in C. (H) TEMPOL pretreatment abolishes 2.5 mM H₂O₂-induced nanopore formation, quantified from scanning electron micrographs. (I) TEMPOL pretreatment diminishes ionizing radiation-induced nanopore formation, quantified from scanning electron micrographs. In C–E and G–I, data represent mean \pm SEM and are derived from 25 cells per group; *, $P < 0.05$; **, $P < 0.01$; ***, $P < 0.001$; ****, $P < 0.0001$, two-tailed Student's *t* test versus 0 Gy (C, E, and I), 0 min (D), control (G), or 0 mM H₂O₂ (H). In A, B, and F, scale bar: 1 μ m. Inset magnification 2 \times .

from those observed with ionizing radiation (Fig. 5 F). H₂O₂-induced membrane nanopores formed in a dose dependent manner, with 1 mM H₂O₂ exposure generating a number of nanopores comparable to 10 Gy at 1 min (8.25 ± 1.6 vs. 5.7 ± 0.9 , mean \pm SEM, respectively; Fig. 5 G). H₂O₂ also induced Cr-51 release, as observed with ionizing radiation exposure (Fig. S4). Pretreating cells for 30 min with 10 mM TEMPOL completely inhibited formation of H₂O₂-induced plasma membrane nanopores (Fig. 5 H). Similarly, 10 mM TEMPOL blocked radiation-induced membrane disruptions following 10 Gy, but only partially blocked their formation at higher radiation doses (Fig. 5 I). We believe that residual membrane nanopore formation at higher doses of ionizing radiation in the presence of TEMPOL is due to direct interaction of radiation with biological membrane target molecules at these higher radiation doses, an effect that would not be inhibitable by antioxidant activity.

We confirmed this biology in primary cultures of bovine aortic endothelial cells (BAECs), which also demonstrate ASMase dependence for apoptosis induction in response to diverse stimuli including ionizing radiation, Fas death receptor activation, and gemcitabine (Jin et al., 2008; Rotolo et al., 2012; van Hell et al., 2017). Notably, Fas death receptor activation in BAECs also induces a lysosomal exocytosis event implicated in activation of the ASMase response (Xu et al., 2012). Previous studies show that ionizing radiation induces CRP formation at the plasma membrane in BAECs within minutes, and apoptosis within hours, both inhibitable by anti-ceramide antibody pretreatment, comparable to the data reported above in Jurkat cells (Rotolo et al., 2012; Stancevic et al., 2013; Truman et al., 2010). Here, we investigated the events proximal to this biology in BAECs and found that ionizing radiation induces plasma membrane nanopores of similar structure, size (155.2 ± 8.0 nm, mean \pm SEM), and dose dependence as in Jurkat cells (Fig. S5, A and B). Furthermore, radiation-induced nanopore formation in BAECs, as in Jurkat cells, is followed by rapid lysosomal exocytosis and apoptosis, events inhibitable by BEL pretreatment (Fig. S5, C and D).

Collectively, these data provide the first mechanistic understanding of initiation of radiation-induced ASMase signaling of apoptotic death. Fig. 6 summarizes the membrane-based, ASMase-mediated apoptotic death pathway described in this study: Ionizing radiation, via oxidation of H₂O, induces lipid peroxidation that yields a full-thickness disruption in the plasma membrane barrier. This nanopore-like structure permits local calcium influx down its concentration gradient, causing fusion within seconds of lysosomes with the plasma membrane. ASMase released by this process hydrolyzes sphingomyelin preferentially concentrated in glycosphingolipid-enriched microdomains ("rafts") on the cell surface, generating ceramide. Ceramide, due to its biophysical properties, spontaneously coalesces into CRPs, sites of protein insertion for the purpose of oligomerization for transmembrane signaling of the stress response, and induction of apoptotic death.

Discussion

Formation of free radicals following radiolysis of water molecules is the primary mechanism of DNA damage to eukaryotes,

leading to mitotic catastrophe and cell death (Hall and Giaccia, 2012). Therapeutic induction of this biology is the principle behind the clinical use of ionizing radiation for treatment of human disease. In this paper, we report that the same biophysical event, i.e., radiolysis of water, yields a form of membrane damage, which, in specific cells, initiates a signal transduction pathway leading to cell death by apoptosis. In this context, radiation-induced nanopore-like structures represent an interaction between radiation-induced ROS and biological molecules that is analogous to that conferring DNA DSBs. As generation of DSBs is a biophysical event, all cells incur the same number of DSBs per dose delivered (assuming normoxia), and hence outcome depends on the cell type capacity and fidelity of the DNA repair apparatus to cure those breaks (Foray et al., 1997; Jeggo and Löbrich, 2015; Powell and McMillan, 1994). We posit that radiation-induced nanopore formation, also a biophysical event, will be similarly dose dependent in mammalian cells, while outcome will depend on the intensity of subsequent ASMase/ceramide signaling, an event widely acknowledged as highly cell type specific. In this context, endothelial cells are highly prone to this membrane-based form of radiation-induced apoptosis (Haimovitz-Friedman et al., 1994; Santana et al., 1996), as they display as much as 20-fold more secreted ASMase than other mammalian cells (Marathe et al., 1998). Ultimately, determination of the extent to which radiation-induced human disease and/or therapy relates to nanopore generation and ASMase-mediated CRPs, and whether this system can be engaged pharmacologically, will require substantial additional investigation.

We have used several independent techniques in an effort to demonstrate that the nanopore-like features we observed by electron microscopy represent disruptions that span the entire width of the plasma membrane. While data using these techniques are indicative of a full-thickness plasma membrane disruption, analogous to that of SLO, which promotes local calcium influx to stimulate fusion of lysosomes to plasma membrane, we acknowledge that results here are not definitive for identification of the nanopore-like structure we observed by electron microscopy as the full-thickness disruptions identified biochemically. In an attempt to provide biophysical evidence for this concept, we employed focused ion beam scanning electron microscopy (FIB-SEM), a sample manipulation and imaging technology nascent in biological applications (Narayan and Subramaniam, 2015). FIB-SEM uses a gallium ion beam to remove layers of a biological sample to reveal underlying structure. Unfortunately, the nanopores were too small a feature for the gallium beam to properly dissect for inspection, as any attempt to expose underlying structure ablated the entire site (unpublished data). We believe that as technologies such as FIB-SEM continue to develop, it may become possible to make the direct observation that the nanopores we observed are full-thickness membrane disruptions. Furthermore, while we hypothesize that cells featuring increased nanopore formation following radiation exposure represent the cell population that will ultimately progress to apoptosis, current technological limitations do not allow us to investigate this progression on a single-cell level.

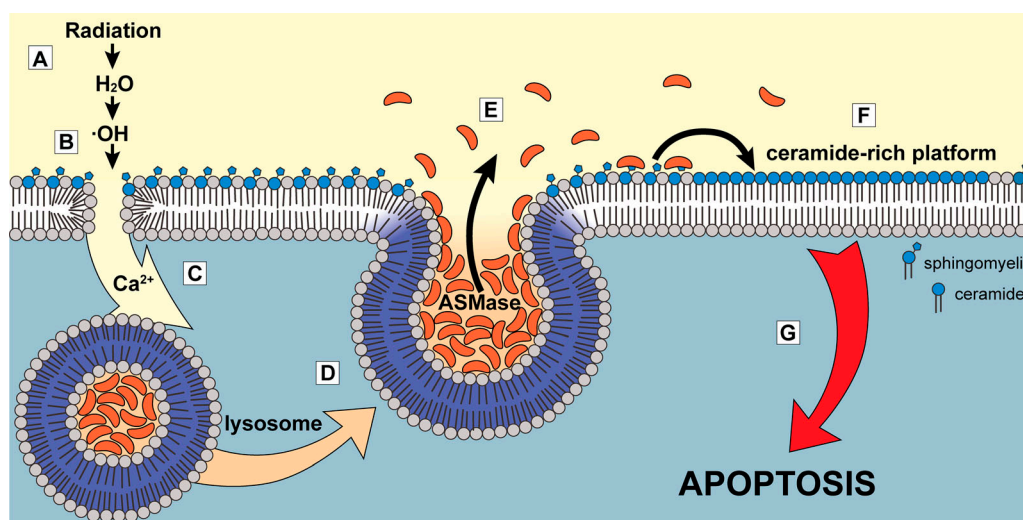


Figure 6. **Model of calcium-dependent ASMase response to ionizing radiation mediated by plasma membrane damage.** (A) Ionizing radiation leads to formation of free radicals via radiolysis of water molecules. (B) Oxidative attack on plasma membrane lipids promotes increased membrane permeability due to increased lipid peroxidation. (C) Calcium ions flow down their concentration gradient into the cell. (D and E) Lysosomes fuse with plasma membrane in a calcium-dependent manner (D), releasing their content (including ASMase) to the cell surface (E). (F) ASMase generates large quantities of ceramide that self-associate to form CRPs. (G) CRPs amplify apoptotic signaling, leading to apoptotic cell death.

To our knowledge, the current studies represent the first description of a cell death mechanism initiated by ionizing radiation-induced physical damage driven by lysosome fusion with plasma membrane. This is not surprising as the literature regarding biological functions of lysosome secretion is relatively new and small. Studies in this report may also address a conundrum in the field of sphingolipid-induced cell death, as numerous stresses, including UV, shear stress, ionizing radiation, select chemotherapeutics (daunorubicin, etoposide, gemcitabine, taxol, etc.), flow stress, and heat stress, have repeatedly been shown to activate ASMase signaling to induce apoptotic death in diverse cells, without any apparent commonality of action (Stancevic and Kolesnick, 2010; Verheij et al., 1996). In this context, we posit that nanopore-mediated lysosome induction of cell death will prove to be a fundamental mechanism of signaling of apoptosis engaged by physical damage to membranes of select cells and will prove pharmacologically tractable for the purposes of radiation sensitization and treatment of microvascular dysfunction that accompanies many metabolic diseases.

Materials and methods

Materials

Bisbenzimidazole trihydrochloride (Hoechst 33258), imipramine hydrochloride (I7379), (\pm)- α -tocopherol (T3251), lipid peroxidation (MDA) assay kit (MAK085), 4-methylumbelliferyl *N*-acetyl- β -D-glucosaminide (M2133), donkey serum (D9663), poly-L-lysine (P1274), BEL (B1552), normal mouse serum (M5905), and TEMPOL (I76141) were purchased from Sigma-Aldrich. [*N*-methyl- 14 C]sphingomyelin (NEC663010uc) and Cr-51 (NEZ030S001MC) were from PerkinElmer. Amicon Ultra-4 Centrifugal Filters (UFC803024) were from EMD Millipore. Anti-ceramide MID 15B4 (ALX-804-196-T050) was from Enzo

Life Sciences. Anti-LAMP-1 (H4A3) conjugated with PE and FITC (sc-20011) were from Santa Cruz Biotechnology. FM 1-43 dye (T3163), Gibco RPMI 1640 medium (11875), Alexa Fluor 488 donkey anti-rabbit IgG (A-21206), Gibco charcoal-stripped FBS (12676-011), BAPTA-AM (B1205), PI (F1930), Gibco charcoal-stripped FBS (12676-011), and 30% hydrogen peroxide (H325) were from Thermo Fisher Scientific. FBS (100-106) was from Gemini Bio-Products. PFA 2%/glutaraldehyde 2.5% in 0.75 M sodium cacodylate buffer (pH 7.5) was from Electron Microscopy Sciences. CyTM3 AffiniPure goat anti-mouse IgG (115-165-003) was from Jackson ImmunoResearch. The CytoTox96 Non-Radioactive Cytotoxicity Assay kit (G1780) for measuring LDH release was from Promega. Pitstop 2 (*N*-[5-(4-bromobenzylidene)-4-oxo-4,5-dihydro-1,3-thiazol-2-yl]naphthalene-1-sulfonamide; ab120687) was from Abcam. Vectashield mounting medium with DAPI (H-1200) was from Vector Labs. Rabbit polyclonal anti-ASMase antibody #1598 was generated against full-length FLAG-tagged human ASMase protein as described (Rotolo et al., 2005). Anti-ceramide 2A2 antibody was purchased from Antibody Research.

Cell culture and stimulation

Jurkat T lymphocytes clone E6-1 (TIB-152, ATCC) were grown in a 5% CO₂ incubator at 37°C in RPMI 1640 supplemented with 10% heat-inactivated FBS. Before stimulation, cells were washed with and suspended in empty RPMI 1640 or supplemented with either 1% FBS or heat-inactivated delipidated FBS and allowed to rest for 15 min to 2 h at 37°C. Cells were then either treated with H₂O₂ or irradiated using a Shepherd Mark-I unit (Model 68; SN643) 137 Cs source irradiator at dose rates of 10 or 1.6 Gy/min. Where indicated, cells were pretreated with imipramine, TEMPOL, α -tocopherol, BAPTA-AM, or anti-ceramide h2A2 before stimulation. Primary BAECs were isolated from the intima of bovine aorta as described (Gospodarowicz et al., 1976)

and cultured in DMEM (HyClone, GE Healthcare) + 10% bovine calf serum (GemCell, Gemini Bio-Products). The day before stimulation, medium was replaced with that containing 0.2% human albumin.

ASMase activity assay

ASMase activity was assayed by radioenzymatic assay using [*N*-methyl-¹⁴C]sphingomyelin substrate as described previously with modification (Rotolo et al., 2005; van Hell et al., 2017). Jurkat cells were resuspended in empty RPMI 1640, irradiated, cold-shocked with ice-cold PBS at indicated times, and placed on ice. Cells were centrifuged at 150 *g* for 5 min in a 4°C centrifuge. Supernatant was collected and centrifuged again to clear cells and debris. Supernatant was concentrated using Amicon Ultra-4 centrifugal filters (UFC803024, EMD Millipore) at 3,200 *g* for 15 min at 4°C. Concentrated cell supernatant was assayed for ASMase activity in 50 mM sodium acetate, pH 5.0, supplemented with 0.1 mM ZnCl₂, 1 mM EDTA, and 0.1% Triton X-100 in the presence of substrate. Reactions were terminated after 2 h with 2:1 CHCl₃:MeOH (vol/vol), and the radiolabeled product was quantified using a scintillation counter (Packard 2200CA Tri-Carb Liquid Scintillation Analyzer). Total activity was calculated based on volume of concentrate.

Ceramide generation

For studies measuring ceramide levels, the diacylglycerol kinase assay was used as previously described (Rotolo et al., 2005). Jurkat cells were passaged 24 times before experiments. On the day of an experiment, Jurkat cells were washed once with Hepes-buffered saline (H/S; 132 mM NaCl, 20 mM Hepes, pH 7.4, 5 mM KCl, 1 mM CaCl₂, 0.7 mM MgCl₂, and 0.8 mM MgSO₄) at 37°C, and 2 × 10⁶ cells were resuspended into 600 μl H/S. Cells were rested for 8–10 min and then exposed to ionizing radiation at 12.5 Gy/min. Stimulation was terminated by addition of 2 ml of chloroform:methanol:1 N HCl (100:100:1, vol/vol/vol), and ceramide was quantified by the diacylglycerol kinase assay.

CRP detection

Platforms were detected as described previously (Rotolo et al., 2005). Briefly, Jurkat cells were resuspended in RPMI 1640 supplemented with 1% heat-inactivated delipidated FBS, irradiated, and fixed in 2% PFA at appropriate times following exposure. Cells were blocked in 2% donkey serum in PBS on ice for 1 h, washed, and resuspended in 1:50 α-ceramide MID 15B4 (ALX-804-196-T050, Enzo Life Sciences) in PBS for 2 h. Cells were then washed with PBS + 0.1% Tween, resuspended in 1:300 CyTM3 AffiniPure goat anti-mouse IgG (H+L) in PBS + 0.1% Tween, and incubated for 1 h on ice. Cells were washed in PBS + 0.1% Tween and mounted on glass slides using Vectashield fluorescent mounting medium containing DAPI (Vector Laboratories). Platforms were imaged on a Leica SP5 Upright confocal microscope with HyD hybrid detector photon counter and HCX PL APO CS 40.0× 1.25 oil UV objective lens at room temperature. Acquisition was performed using Leica LAS AF software and counting of images with ImageJ v2.0 (National Institutes of Health). Platforms were quantified as percentage of cells exhibiting

platform staining as indicated by condensed fluorescence to ~25% of cell circumference.

ASMase surface translocation

Jurkat cells were irradiated and fixed in 2% PFA for 10 min. Cells were then washed in PBS and blocked in 2% donkey serum in PBS for 2 h. Primary staining was performed with rabbit polyclonal α-ASMase 1598 (1:100) in PBS overnight at 4°C. Cells were washed again, and secondary staining was performed with Alexa Fluor 488 donkey anti-rabbit IgG (1:750). Cells were washed again with PBS, resuspended in Vectashield mounting medium with DAPI, and imaged using a Zeiss Imager Z2 widefield microscope with Zeiss Plan-Apochromat 20×/0.8 objective lens and Zeiss Axiocam 506 Mono camera at room temperature. Acquisition was performed using Zeiss Zen Blue software and counting of images with ImageJ v2.0.

Apoptosis assay

Apoptosis was assessed as described previously (Rotolo et al., 2005). Jurkat cells were resuspended in RPMI 1640 supplemented with 1% FBS, irradiated, incubated at 37°C, and fixed with 2% PFA at the appropriate time. Cells were then washed with PBS and stained with 24 μg/ml bisbenzimidazole trihydrochloride (Hoechst 33258; Sigma-Aldrich) and placed on glass slides for counting on an Olympus IMT-2 microscope using a 40× DPlanApo40UV 0.850160/0.11–0.23 objective lens at room temperature. For BAEC apoptosis, cells were washed into 0.2% human serum albumin DMEM, irradiated, and incubated at 37°C for the indicated time. Cells were trypsinized and fixed, followed by staining with bisbenzimidazole hydrochloride. Apoptosis was counted based on morphological characteristics of apoptotic nuclei, including chromatin condensation, segmentation, and compaction along with nuclear periphery and appearance of apoptotic bodies, using a fluorescence microscope. A minimum of 100 cells was counted per sample.

LAMP1 surface staining

Surface expression of LAMP1 was assayed as described previously, with modification (Reddy et al., 2001). Jurkat cells at 4°C were irradiated, transferred to a 37°C water bath for the indicated times, and placed on ice. Cells were blocked in 2% normal mouse serum (M5905, Sigma-Aldrich) in PBS for 10 min, centrifuged, and stained with 1:250 α-LAMP1 H4A3 (sc-20011, Santa Cruz Biotechnology) in 2% normal mouse serum in PBS for 60 min. Stained cells were then washed and fixed in 2% PFA for 10 min. After fixing, cells were washed and mounted on poly-L-lysine-coated glass slides using Vectashield fluorescent mounting medium containing DAPI (Vector Laboratories) for confocal imaging. Surface staining was imaged on a Leica SP5 Upright confocal microscope with HyD detector and HCX PL APO CS 40.0× 1.25 oil UV objective lens at room temperature. Acquisition was performed using Leica LAS AF software and analysis of surface area staining with ImageJ v2.0.

β-Hexosaminidase secretion assay

Secreted β-hexosaminidase activity was measured in a manner similar to secreted ASMase activity as described above. Jurkat

cells were irradiated, incubated at 37°C for 2 min, and cold-shocked with ice-cold PBS. Cells were then centrifuged at 150 *g* for 5 min at 4°C. Supernatant was concentrated in the same manner as the secreted ASMase activity assay, and cell pellets were lysed in 0.1% Triton X-100. Supernatant and lysate samples were incubated with 2 mM fluorescent substrate 4-methylumbelliferyl *N*-acetyl- β -D-glucosaminide in citrate/sodium phosphate, pH 4.5, in a 96-well plate at 37°C for 90 min. Reactions were quenched with 267 mM glycine, pH 11.0, and fluorescence intensity was assayed at 362-nm excitation and 448-nm emission to measure 4-methylumbelliferone product.

Cell permeability assay

PI (F1930, Thermo Fisher Scientific) influx was used to measure plasma membrane permeabilization as described (Idone et al., 2008). Jurkat cells were resuspended in RPMI 1640 with and without calcium (with 1 mM EDTA supplementation in medium without calcium), and 100 \times PI was added immediately before irradiation. Cells were immediately placed on ice, mounted, and imaged for PI uptake by fluorescence microscopy on a Zeiss Imager Z2 wide-field microscope with a Zeiss Plan-Apochromat 20 \times /0.8 objective lens and Zeiss AxioCam 506 Mono camera at room temperature. Acquisition was performed using Zeiss Zen Blue software and counting of images with ImageJ v2.0. Alternatively, influx of the lipophilic dye FM 1-43 was used as previously described (Tam et al., 2013). Cells were washed into PBS + Ca²⁺ and allowed to attach to poly-L-lysine-coated chamber glass slides (LabTek #1.5 German borosilicate, 155382, Thermo Fisher Scientific). Cells were then placed on ice and washed with calcium-free PBS + 2 mM EDTA, and 4 μ M FM 1-43 in PBS – Ca²⁺ was added. Cells were immediately irradiated, placed back on ice, and imaged on a Zeiss LSM 880 confocal microscope on an AxioObserver inverted stand (Carl Zeiss), using a 63 \times /1.4NA objective with optical zoom of 2 \times . To minimize the internalization of the FM 1-43 dye, the sample was placed on a temperature-controlled stage insert, which was maintained at 4°C (Julabo F25). Brightfield and FM 1-43 channels were imaged with a 488-nm argon laser, and emitted fluorescence was captured in the ~540–650-nm range. A series of 5 \times 5 tile scans of a single optical slice through the cells were captured to image more cells in rapid succession. Analysis of intracellular signal integrated density was performed with ImageJ v2.0. Additionally, cell permeabilization was measured by release of Cr-51 from prelabeled Jurkat T cells. Briefly, 5 \times 10⁵ cells were loaded with 80 μ Ci Cr-51 activity for 90 min and resuspended in calcium-free PBS + 2 mM EDTA. Cells were irradiated as described and centrifuged, and the supernatant was collected and counted using a TopCount NXT scintillation counter (Packard). To measure LDH release, cells were washed with PBS – Ca²⁺, resuspended in PBS + 2 mM EDTA, and immediately irradiated. Cells were placed on ice at indicated time points and then centrifuged. LDH activity in sample supernatants was detected using the CytoTox96 Non-Radioactive Cytotoxicity Assay (G1780, Promega), measuring the formazan reaction product at 490-nm absorbance as per vendor instructions.

Lipid peroxidation (MDA) assay

Lipid peroxidation was quantified using a thiobarbituric acid assay that measures MDA (MAK085, Sigma-Aldrich) as per vendor instructions. Cells were irradiated, immediately placed on ice, and centrifuged at 300 *g* for 5 min at 4°C. Supernatant was aspirated and discarded, and cell pellet was lysed in the presence of butylated hydroxytoluene for 1 h. Protein was then precipitated by adding HClO₄ to 5.5% final and centrifuging at 13,000 *g* for 10 min. Supernatant was reacted with thiobarbituric acid at 95°C for 1 h, and MDA content was measured via fluorescence at excitation 532/emission 553 nm.

Scanning electron microscopy

For detection of cell surface disruptions, Jurkat cells were prepared for scanning electron microscopy imaging following stimulation. Thermanox coverslips were coated with poly-L-lysine overnight and gently rinsed and dried the next day. Coated coverslips were then placed in 35 \times 10-mm dishes. Cells were washed in and resuspended in PBS, transferred to dishes with coverslips, and allowed to attach for 15 min at room temperature. Cells were then irradiated and fixed with PFA 2%/glutaraldehyde 2.5% in 0.75 M sodium cacodylate buffer (pH 7.5; Electron Microscopy Sciences) at appropriate times. Samples were then dehydrated through a graded series of alcohol (50, 75, 95, and 100% alcohol) and critical point dried in a Denton Critical Point Drying Apparatus JCP1 followed by coating of gold/palladium in a Denton Vacuum DeskIV Sputter coater. Imaging was performed with Zeiss Supra 25 and Hitachi S340 Field Emission scanning electron microscopes. Quantification of cell surface disruptions was performed by counting disruption-like features of \geq 100 nm in diameter visible on the top hemisphere of the cell. A minimum of 25 cells was imaged for counting per sample.

Statistical analysis

Statistical analysis was performed using GraphPad Prism software v7 using two-tailed Student's *t* test with 95% confidence limits. *, *P* < 0.05; **, *P* < 0.01; ***, *P* < 0.001; and ****, *P* < 0.0001 were considered significant. Normality of data distribution was not tested but was assumed to be normal.

Online supplemental material

Fig. S1 demonstrates the protective effects of anti-ceramide antibody h2A2, ASMase inhibitor imipramine, and lysosomal exocytosis inhibitor BEL against radiation-induced apoptosis in Jurkat cells. Fig. S2 shows the inhibitory effect of extracellular calcium removal on radiation-induced lysosomal exocytosis. Fig. S3 characterizes the influx of FM 1-43 dye into cells following radiation exposure. Fig. S4 shows the plasma membrane-damaging effects of H₂O₂. Fig. S5 includes nanopore scanning electron microscopy imaging/quantification, lysosomal exocytosis, and BEL protection against apoptosis following radiation exposure of BAECs.

Acknowledgments

Scanning electron microscopy was performed with support of Nina Lampen and the SKI Electron Microscopy Core Facility and

the EM services of the Microscopy and Image Analysis Core of Weill Cornell Medicine and the Department of Pathology of Icahn School of Medicine at Mount Sinai. Confocal microscopy was performed with support of the MSKCC Molecular Cytology Core Facility.

This work was supported by funds and a gift from the Virginia and D.K. Ludwig Fund for Cancer Research (Z. Fuks). This research was funded in part through the National Institutes of Health/National Cancer Institute Cancer Center Support Core Grant P30 CA008748 and by National Institutes of Health predoctoral training grants 5T32GM073546-07 and 5T32GM073546-08. Microscopy services were provided by the MSKCC Molecular Cytology Core Facility (National Cancer Institute Core Grant P30 CA008748). Referenced FIB-SEM work was performed at the Simons Electron Microscopy Center and National Resource for Automated Molecular Microscopy located at the New York Structural Biology Center with the help of Ashleigh Raczkowski and Ed Eng, supported by grants from the Simons Foundation (SF349247), NYSTAR, and the National Institutes of Health/National Institute of General Medical Sciences (GM103310) with additional support from National Institutes of Health grant S10 RR029300-01.

Some authors hold patents unrelated to this work: US7195775B1, US7850984B2, and US10052387B2 (R.N. Kolesnick); US8562993B2, US9592238B2, US20150216971A1, and US20170335014A1 (R.N. Kolesnick and J.A. Rotolo); and US20170333413A1 and US20180015183A1 (R.N. Kolesnick and Z. Fuks). R.N. Kolesnick and Z. Fuks are cofounders of Ceramedix Holding LLC. The authors declare no further competing financial interests.

Author contributions: C.S. Ferranti, J. Cheng, C. Thompson, J. Zhang, J.A. Rotolo, and S. Buddaseth conducted investigation, developed methodology, and performed formal analysis of data. C.S. Ferranti and R.N. Kolesnick wrote the manuscript; Z. Fuks and R.N. Kolesnick provided overall scientific direction and supervision.

Submitted: 4 April 2019

Revised: 23 December 2019

Accepted: 5 February 2020

References

- Beckmann, N., D. Sharma, E. Gulbins, K.A. Becker, and B. Edelmann. 2014. Inhibition of acid sphingomyelinase by tricyclic antidepressants and analogs. *Front. Physiol.* 5:331. <https://doi.org/10.3389/fphys.2014.00331>
- Belka, C., C. Gruber, V. Jendrossek, S. Wesselborg, and W. Budach. 2003. The tyrosine kinase Lck is involved in regulation of mitochondrial apoptosis pathways. *Oncogene*. 22:176–185. <https://doi.org/10.1038/sj.onc.1206103>
- Belka, C., P. Marini, A. Lepple-Wienhues, W. Budach, A. Jekle, M. Los, F. Lang, K. Schulze-Osthoff, E. Gulbins, and M. Bamberg. 1999. The tyrosine kinase lck is required for CD95-independent caspase-8 activation and apoptosis in response to ionizing radiation. *Oncogene*. 18:4983–4992. <https://doi.org/10.1038/sj.onc.1202878>
- Boesen-de Cock, J.G., A.D. Tepper, E. de Vries, W.J. van Blitterswijk, and J. Borst. 1999. Common regulation of apoptosis signaling induced by CD95 and the DNA-damaging stimuli etoposide and γ -radiation downstream from caspase-8 activation. *J. Biol. Chem.* 274:14255–14261. <https://doi.org/10.1074/jbc.274.20.14255>

- Bordenave, L., R. Bareille, F. Lefebvre, and C. Baquay. 1993. A Comparison between ^{51}Cr Release and LDH Release to Measure Cell Membrane Integrity: Interest for Cytocompatibility Studies with Biomaterials. *J. Appl. Biomater.* 4:309–315. <https://doi.org/10.1002/jab.770040405>
- Charruyer, A., S. Grazide, C. Bezombes, S. Müller, G. Laurent, and J.P. Jaffrézou. 2005. UV-C light induces raft-associated acid sphingomyelinase and JNK activation and translocation independently on a nuclear signal. *J. Biol. Chem.* 280:19196–19204. <https://doi.org/10.1074/jbc.M412867200>
- Cremesti, A., F. Paris, H. Grassmé, N. Holler, J. Tschopp, Z. Fuks, E. Gulbins, and R. Kolesnick. 2001. Ceramide enables fas to cap and kill. *J. Biol. Chem.* 276:23954–23961. <https://doi.org/10.1074/jbc.M101866200>
- Czibener, C., N.M. Sherer, S.M. Becker, M. Pypaert, E. Hui, E.R. Chapman, W. Mothes, and N.W. Andrews. 2006. Ca^{2+} and synaptotagmin VII-dependent delivery of lysosomal membrane to nascent phagosomes. *J. Cell Biol.* 174:997–1007. <https://doi.org/10.1083/jcb.200605004>
- Defour, A., J.H. Van der Meulen, R. Bhat, A. Bigot, R. Bashir, K. Nagaraju, and J.K. Jaiswal. 2014. Dysferlin regulates cell membrane repair by facilitating injury-triggered acid sphingomyelinase secretion. *Cell Death Dis.* 5:e1306. <https://doi.org/10.1038/cddis.2014.272>
- Dumitru, C.A., and E. Gulbins. 2006. TRAIL activates acid sphingomyelinase via a redox mechanism and releases ceramide to trigger apoptosis. *Oncogene*. 25:5612–5625. <https://doi.org/10.1038/sj.onc.1209568>
- Dutta, D., C.D. Williamson, N.B. Cole, and J.G. Donaldson. 2012. Pitstop 2 is a potent inhibitor of clathrin-independent endocytosis. *PLoS One*. 7:e45799. <https://doi.org/10.1371/journal.pone.0045799>
- Foray, N., C.F. Arlett, and E.P. Malaise. 1997. Radiation-induced DNA double-strand breaks and the radiosensitivity of human cells: a closer look. *Biochimie*. 79:567–575. [https://doi.org/10.1016/S0300-9084\(97\)82005-6](https://doi.org/10.1016/S0300-9084(97)82005-6)
- Garcia-Barros, M., F. Paris, C. Cordon-Cardo, D. Lyden, S. Rafii, A. Haimovitz-Friedman, Z. Fuks, and R. Kolesnick. 2003. Tumor response to radiotherapy regulated by endothelial cell apoptosis. *Science*. 300:1155–1159. <https://doi.org/10.1126/science.1082504>
- Gospodarowicz, D., J. Moran, D. Braun, and C. Birdwell. 1976. Clonal growth of bovine vascular endothelial cells: fibroblast growth factor as a survival agent. *Proc. Natl. Acad. Sci. USA*. 73:4120–4124. <https://doi.org/10.1073/pnas.73.11.4120>
- Grassme, H., A. Jekle, A. Riehle, H. Schwarz, J. Berger, K. Sandhoff, R. Kolesnick, and E. Gulbins. 2001. CD95 signaling via ceramide-rich membrane rafts. *J. Biol. Chem.* 276:20589–20596. <https://doi.org/10.1074/jbc.M101207200>
- Grassmé, H., A. Cremesti, R. Kolesnick, and E. Gulbins. 2003. Ceramide-mediated clustering is required for CD95-DISC formation. *Oncogene*. 22:5457–5470. <https://doi.org/10.1038/sj.onc.1206540>
- Grassmé, H., V. Jendrossek, J. Bock, A. Riehle, and E. Gulbins. 2002. Ceramide-rich membrane rafts mediate CD40 clustering. *J. Immunol.* 168:298–307. <https://doi.org/10.4049/jimmunol.168.1.298>
- Hahn, S.M., C.M. Krishna, A. Samuni, W. DeGraff, D.O. Cuscenza, P. Johnstone, and J.B. Mitchell. 1994. Potential use of nitroxides in radiation oncology. *Cancer Res.* 54(7 suppl):2006s–2010s.
- Haimovitz-Friedman, A., C.C. Kan, D. Ehleiter, R.S. Persaud, M. McLoughlin, Z. Fuks, and R.N. Kolesnick. 1994. Ionizing radiation acts on cellular membranes to generate ceramide and initiate apoptosis. *J. Exp. Med.* 180:525–535. <https://doi.org/10.1084/jem.180.2.525>
- Hall, E.J., and A.J. Giaccia. 2012. Radiobiology for the Radiobiologist. Seventh edition. Lippincott Williams & Wilkins, Philadelphia, PA.
- Holopainen, J.M., M.I. Angelova, and P.K. Kinnunen. 2000. Vectorial budding of vesicles by asymmetrical enzymatic formation of ceramide in giant liposomes. *Biophys. J.* 78:830–838. [https://doi.org/10.1016/S0006-3495\(00\)76640-9](https://doi.org/10.1016/S0006-3495(00)76640-9)
- Howard, A.C., A.K. McNeil, and P.L. McNeil. 2011. Promotion of plasma membrane repair by vitamin E. *Nat. Commun.* 2:597. <https://doi.org/10.1038/ncomms1594>
- Idone, V., C. Tam, J.W. Goss, D. Toomre, M. Pypaert, and N.W. Andrews. 2008. Repair of injured plasma membrane by rapid Ca^{2+} -dependent endocytosis. *J. Cell Biol.* 180:905–914. <https://doi.org/10.1083/jcb.200708010>
- Jeggo, P.A., and M. Löbrich. 2015. How cancer cells hijack DNA double-strand break repair pathways to gain genomic instability. *Biochem. J.* 471:1–11. <https://doi.org/10.1042/BJ20150582>
- Jin, S., F. Yi, F. Zhang, J.L. Poklis, and P.L. Li. 2008. Lysosomal targeting and trafficking of acid sphingomyelinase to lipid raft platforms in coronary endothelial cells. *Arterioscler. Thromb. Vasc. Biol.* 28:2056–2062. <https://doi.org/10.1161/ATVBAHA.108.172478>

- LeMotte, P.K., and J.B. Little. 1984. DNA damage induced in human diploid cells by decay of incorporated radionuclides. *Cancer Res.* 44:1337–1342.
- Li, X., E. Gulbins, and Y. Zhang. 2012. Oxidative stress triggers Ca-dependent lysosome trafficking and activation of acid sphingomyelinase. *Cell. Physiol. Biochem.* 30:815–826. <https://doi.org/10.1159/000341460>
- Marathe, S., S.L. Schissel, M.J. Yellin, N. Beatini, R. Mintzer, K.J. Williams, and I. Tabas. 1998. Human vascular endothelial cells are a rich and regulatable source of secretory sphingomyelinase. Implications for early atherogenesis and ceramide-mediated cell signaling. *J. Biol. Chem.* 273:4081–4088. <https://doi.org/10.1074/jbc.273.7.4081>
- Narayan, K., and S. Subramaniam. 2015. Focused ion beams in biology. *Nat. Methods.* 12:1021–1031. <https://doi.org/10.1038/nmeth.3623>
- Nurminen, T.A., J.M. Holopainen, H. Zhao, and P.K.J. Kinnunen. 2002. Observation of topical catalysis by sphingomyelinase coupled to microspheres. *J. Am. Chem. Soc.* 124:12129–12134. <https://doi.org/10.1021/ja017807r>
- Powell, S.N., and T.J. McMillan. 1994. The repair fidelity of restriction enzyme-induced double strand breaks in plasmid DNA correlates with radioresistance in human tumor cell lines. *Int. J. Radiat. Oncol. Biol. Phys.* 29:1035–1040. [https://doi.org/10.1016/0360-3016\(94\)90399-9](https://doi.org/10.1016/0360-3016(94)90399-9)
- Radford, I.R., and G.S. Hodgson. 1985. 125I-induced DNA double strand breaks: use in calibration of the neutral filter elution technique and comparison with X-ray induced breaks. *Int. J. Radiat. Biol. Relat. Stud. Phys. Chem. Med.* 48:555–566. <https://doi.org/10.1080/09553008514551611>
- Reddy, A., E.V. Caler, and N.W. Andrews. 2001. Plasma membrane repair is mediated by Ca(2+)-regulated exocytosis of lysosomes. *Cell.* 106:157–169. [https://doi.org/10.1016/S0092-8674\(01\)00421-4](https://doi.org/10.1016/S0092-8674(01)00421-4)
- Rotolo, J., B. Stancevic, J. Zhang, G. Hua, J. Fuller, X. Yin, A. Haimovitz-Friedman, K. Kim, M. Qian, M. Cardó-Vila, et al. 2012. Anti-ceramide antibody prevents the radiation gastrointestinal syndrome in mice. *J. Clin. Invest.* 122:1786–1790. <https://doi.org/10.1172/JCI59920>
- Rotolo, J.A., J. Zhang, M. Donepudi, H. Lee, Z. Fuks, and R. Kolesnick. 2005. Caspase-dependent and -independent activation of acid sphingomyelinase signaling. *J. Biol. Chem.* 280:26425–26434. <https://doi.org/10.1074/jbc.M414569200>
- Santana, P., L.A. Peña, A. Haimovitz-Friedman, S. Martin, D. Green, M. McLoughlin, C. Cordon-Cardo, E.H. Schuchman, Z. Fuks, and R. Kolesnick. 1996. Acid sphingomyelinase-deficient human lymphoblasts and mice are defective in radiation-induced apoptosis. *Cell.* 86:189–199. [https://doi.org/10.1016/S0092-8674\(00\)80091-4](https://doi.org/10.1016/S0092-8674(00)80091-4)
- Seideman, J.H., B. Stancevic, J.A. Rotolo, M.R. McDevitt, R.W. Howell, R.N. Kolesnick, and D.A. Scheinberg. 2011. Alpha particles induce apoptosis through the sphingomyelin pathway. *Radiat. Res.* 176:434–446. <https://doi.org/10.1667/RR2472.1>
- Singh, V.K., L.A. Beattie, and T.M. Seed. 2013. Vitamin E: tocopherols and tocotrienols as potential radiation countermeasures. *J. Radiat. Res. (Tokyo).* 54:973–988. <https://doi.org/10.1093/jrr/rrt048>
- Stancevic, B., and R. Kolesnick. 2010. Ceramide-rich platforms in transmembrane signaling. *FEBS Lett.* 584:1728–1740. <https://doi.org/10.1016/j.febslet.2010.02.026>
- Stancevic, B., N. Varda-Bloom, J. Cheng, J.D. Fuller, J.A. Rotolo, M. García-Barros, R. Feldman, S. Rao, R.R. Weichselbaum, D. Harats, et al. 2013. Adenoviral transduction of human acid sphingomyelinase into neo-angiogenic endothelium radiosensitizes tumor cure. *PLoS One.* 8: e69025. <https://doi.org/10.1371/journal.pone.0069025>
- Stark, G. 1991. The effect of ionizing radiation on lipid membranes. *Biochim. Biophys. Acta.* 1071:103–122. [https://doi.org/10.1016/0304-4157\(91\)90020-W](https://doi.org/10.1016/0304-4157(91)90020-W)
- Tam, C., A.R. Flannery, and N. Andrews. 2013. Live imaging assay for assessing the roles of Ca²⁺ and sphingomyelinase in the repair of pore-forming toxin wounds. *J. Vis. Exp.* (78):e50531.
- Tam, C., V. Idone, C. Devlin, M.C. Fernandes, A. Flannery, X. He, E. Schuchman, I. Tabas, and N.W. Andrews. 2010. Exocytosis of acid sphingomyelinase by wounded cells promotes endocytosis and plasma membrane repair. *J. Cell Biol.* 189:1027–1038. <https://doi.org/10.1083/jcb.201003053>
- Tepper, A.D., E. de Vries, W.J. van Blitterswijk, and J. Borst. 1999. Ordering of ceramide formation, caspase activation, and mitochondrial changes during CD95- and DNA damage-induced apoptosis. *J. Clin. Invest.* 103: 971–978. <https://doi.org/10.1172/JCI5457>
- Truman, J.P., M. García-Barros, M. Kaag, D. Hambarzumyan, B. Stancevic, M. Chan, Z. Fuks, R. Kolesnick, and A. Haimovitz-Friedman. 2010. Endothelial membrane remodeling is obligate for anti-angiogenic radiosensitization during tumor radiosurgery. *PLoS One.* 5:e12310. <https://doi.org/10.1371/journal.pone.0012310>
- van der Goot, F.G., and T. Harder. 2001. Raft membrane domains: from a liquid-ordered membrane phase to a site of pathogen attack. *Semin. Immunol.* 13:89–97. <https://doi.org/10.1006/smim.2000.0300>
- van Hell, A.J., A. Haimovitz-Friedman, Z. Fuks, W.D. Tap, and R. Kolesnick. 2017. Gemcitabine kills proliferating endothelial cells exclusively via acid sphingomyelinase activation. *Cell. Signal.* 34:86–91. <https://doi.org/10.1016/j.cellsig.2017.02.021>
- Verheij, M., R. Bose, X.H. Lin, B. Yao, W.D. Jarvis, S. Grant, M.J. Birrer, E. Szabo, L.I. Zon, J.M. Kyriakis, et al. 1996. Requirement for ceramide-initiated SAPK/JNK signalling in stress-induced apoptosis. *Nature.* 380: 75–79. <https://doi.org/10.1038/380075a0>
- Vit, J.-P., and F. Rosselli. 2003. Role of the ceramide-signaling pathways in ionizing radiation-induced apoptosis. *Oncogene.* 22:8645–8652. <https://doi.org/10.1038/sj.onc.1207087>
- Xu, M., M. Xia, X.-X. Li, W.-Q. Han, K.M. Boini, F. Zhang, Y. Zhang, J.K. Ritter, and P.-L. Li. 2012. Requirement of translocated lysosomal V1 H(+)-ATPase for activation of membrane acid sphingomyelinase and raft clustering in coronary endothelial cells. *Mol. Biol. Cell.* 23:1546–1557. <https://doi.org/10.1091/mbc.e11-09-0821>

Supplemental material

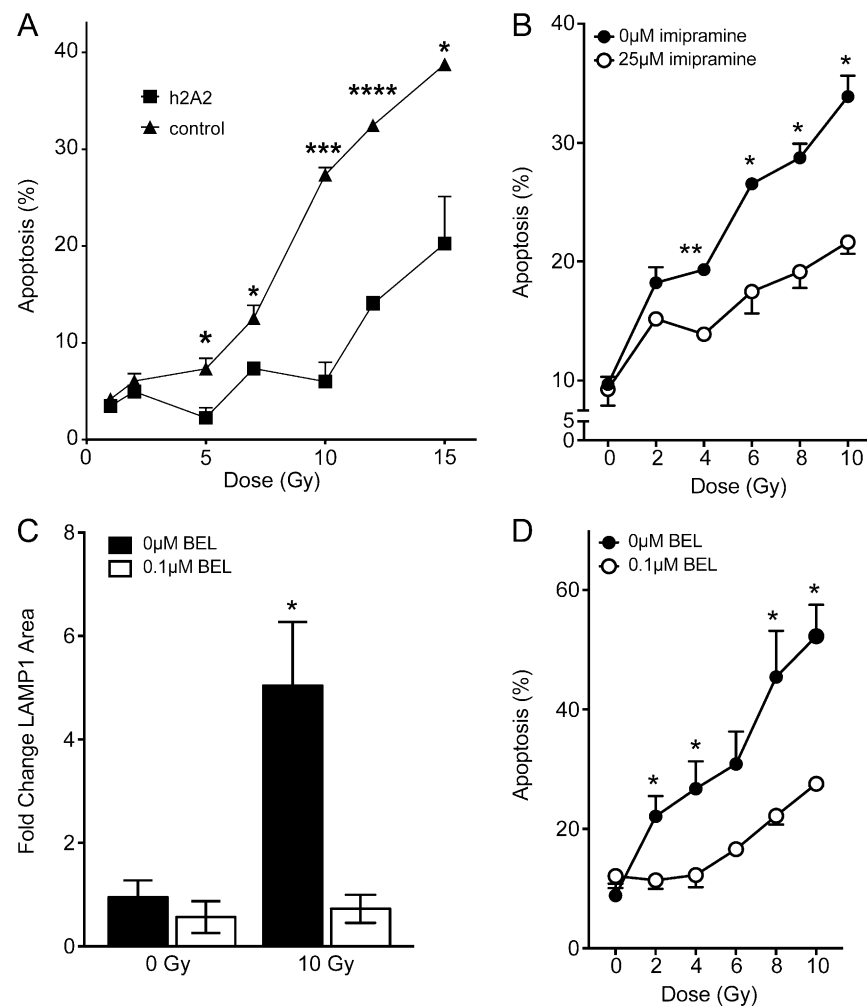


Figure S1. **Inhibition of ceramide signaling and lysosomal exocytosis protect against ionizing radiation-induced apoptosis.** (A) 15-min pretreatment with 10 μ g/ml h2A2 anti-ceramide antibody inhibits 10 Gy-induced apoptosis 16 h following radiation exposure, quantified by bisbenzamide nuclear staining. (B) Inhibition of ASMase by 1-h pretreatment with 25 μ M imipramine blocks radiation dose-dependent apoptotic cell death as measured in A. (C) Pretreatment with the lysosomal exocytosis inhibitor BEL (0.1 μ M) prevents radiation-induced lysosomal exocytosis as measured by LAMP1 surface staining 2 min after radiation exposure. (D) BEL pretreatment inhibits dose-dependent apoptotic death in Jurkat cells as measured in A. Data (mean \pm SEM) are collated from three to four independent experiments. *, $P < 0.05$; **, $P < 0.01$; ***, $P < 0.001$; ****, $P < 0.0001$, two-tailed Student's t test versus h2A2 (A), 25 μ M imipramine (B), untreated control (C), and 0.1 μ M BEL (D).

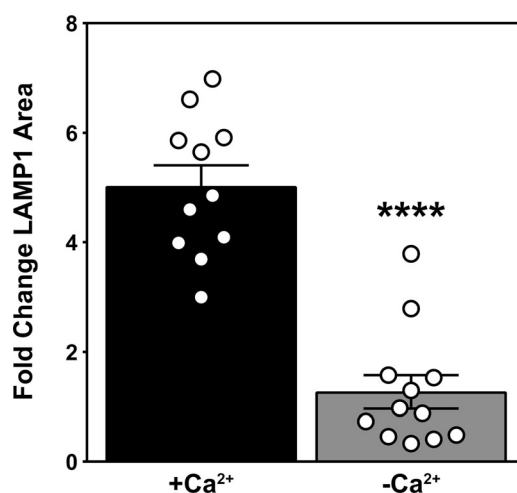


Figure S2. **Depletion of extracellular calcium inhibits ionizing radiation-induced lysosomal exocytosis.** LAMP1 surface staining as detected by anti-LAMP1 antibody 1 min after 10 Gy is inhibited by extracellular calcium removal. Data (mean \pm SEM) are derived from a minimum of 10 cells per group; ****, $P < 0.0001$, two-tailed Student's t test. This experiment was repeated twice with similar results.

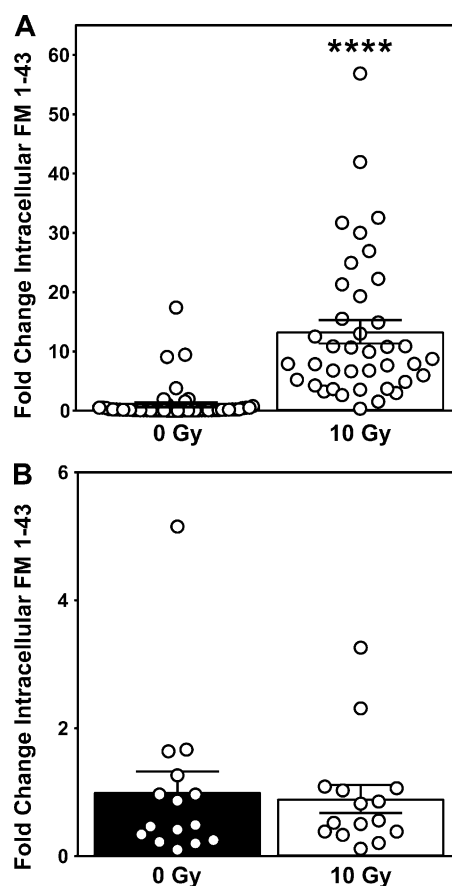


Figure S3. **Ionizing radiation-induced influx of FM 1-43 dye is derived from the extracellular space and not by plasma membrane endocytosis.** (A) Intracellular staining of FM 1-43 immediately following 10-Gy exposure is not blocked by the endocytosis inhibitor pitstop 2 (20 μ M). Data (mean \pm SEM) are derived from a minimum of 39 cells per group; ****, $P < 0.0001$, two-tailed Student's t test. (B) Removal of extracellular FM 1-43 immediately before irradiation abolishes 10 Gy-induced increase of intracellular dye detection. Data (mean \pm SEM) are derived from 15 cells per group.

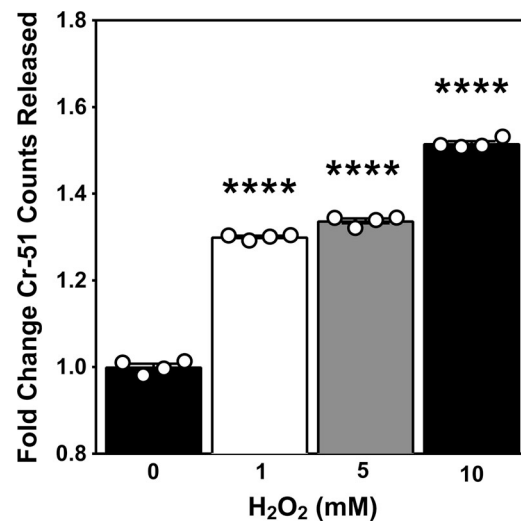


Figure S4. **H₂O₂-induced plasma membrane damage.** Release of preloaded Cr-51 detected in cleared cell medium 2 min following escalating doses of H₂O₂. Data (mean ± SEM) are from four technical replicates; ****, $P < 0.0001$, two-tailed Student's t test. This experiment was repeated twice with similar results.

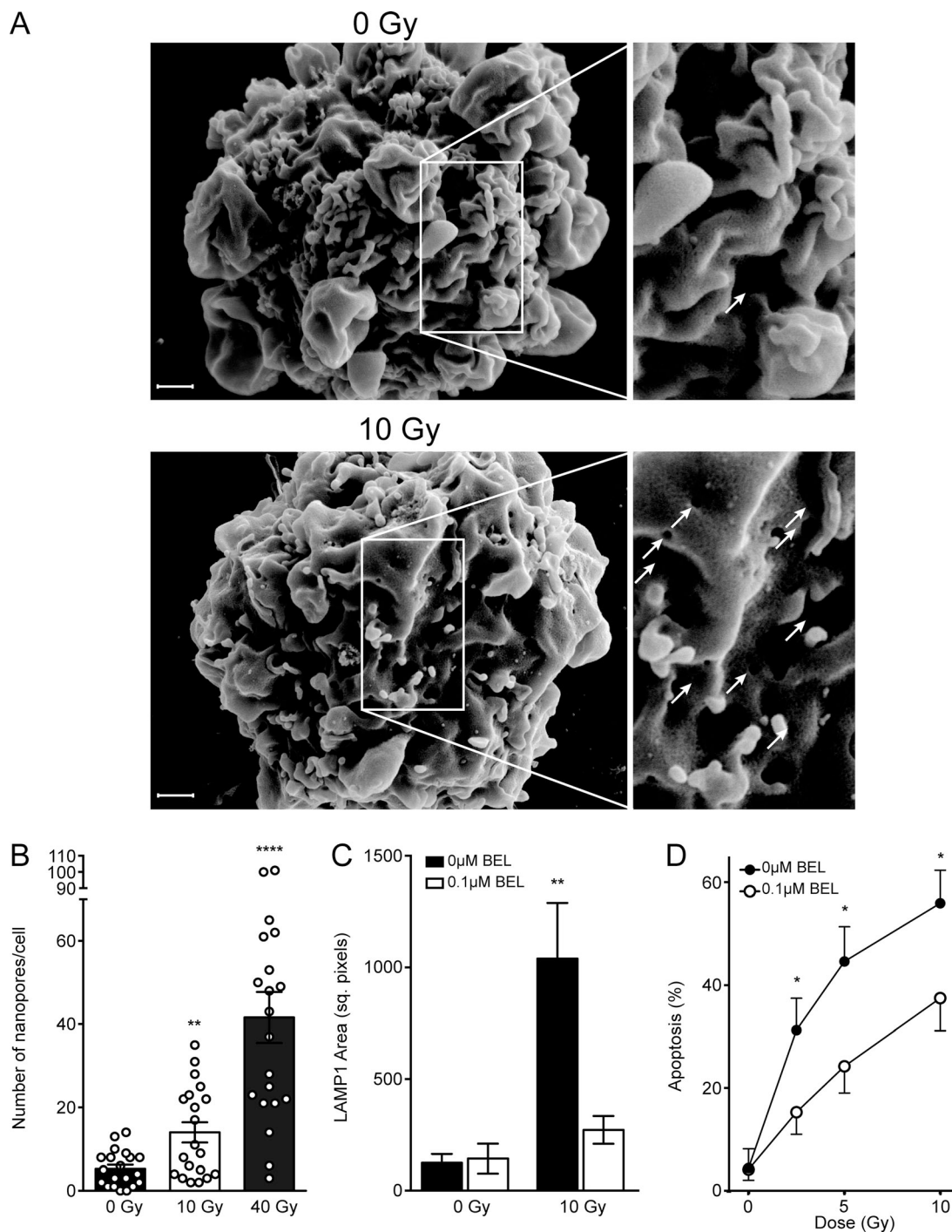


Figure S5. **Radiation induces nanopores and triggers lysosomal exocytosis-mediated apoptosis in BAECs.** (A) Representative scanning electron micrographs of BAEC plasma membrane nanopores (bottom, white arrows in inset) 1 min following 10-Gy exposure. (B) Nanopore formation at 1 min is dose dependent up to 40 Gy, quantified from scanning electron micrographs. (C and D) The lysosomal exocytosis inhibitor BEL blocks LAMP1 surface staining (C) as detected by anti-LAMP1 antibody 2 min after 10 Gy and dose-dependent apoptosis (D) as measured by bisbenzimid staining 8 h after exposure. Note that as the radiation dose escalates, ASMAse-independent DNA damage-mediated death becomes more pronounced, consistent with published literature (Garcia-Barros et al, 2003). Data represent mean \pm SEM (A–C) and mean \pm 95% confidence interval (D) and are derived from 20 cells per group (B), ≥ 7 cells per group (C), and ≥ 200 cells per group (D). **, $P < 0.01$; ****, $P < 0.0001$, two-tailed Student's t test versus 0 Gy control (A–C) and 0 μ M BEL (D). Scale bar: 1 μ m. Inset magnification 2 \times .